IVYSPRING INTERNATIONAL PUBLISHER

Theranostics

2019; 9(3): 778-795. doi: 10.7150/thno.29964

Research Paper

Targeted Drug Delivery and Image-Guided Therapy of Heterogeneous Ovarian Cancer Using HER2-Targeted Theranostic Nanoparticles

Minati Satpathy[1], Liya Wang[2], Rafal J. Zielinski[3], Weiping Qian[1], Y. Andrew Wang[4], Aaron M. Mohs[5], Brad A. Kairdolf[5], Xin Ji[4], Jacek Capala[6], Malgorzata Lipowska[2], Shuming Nie[5], Hui Mao[2], Lily Yang[1]✉

1. Departments of Surgery, Emory University School of Medicine, Atlanta, GA, 30322, USA.
2. Department of Radiology and Imaging Sciences, Emory University School of Medicine, Atlanta, GA, 30322, USA.
3. Department of Experimental Therapeutics, University of Texas, MD Anderson Cancer Center, Houston, TX, 77030, USA.
4. Ocean NanoTech, LLC, San Diego, CA, 92126, USA.
5. Department of Biomedical Engineering, Emory University, Atlanta, GA, 30322, USA.
6. Clinical Radiation Oncology Branch, Division of Cancer Treatment and Diagnosis, National Cancer Institute, Bethesda, MD 20892, USA.

✉ Corresponding author: Dr. Lily Yang, Department of Surgery, Emory University School of Medicine, 1365 C Clifton Road, NE, Atlanta, GA, 30322, USA. Tel: + 1 404-778-4269, Fax: + 1 404-778-5530, Email: lyang02@emory.edu

Received: 2018.09.16; Accepted: 2018.12.19; Published: 2019.01.24

Abstract

Cancer heterogeneity and drug resistance limit the efficacy of cancer therapy. To address this issue, we have developed an integrated treatment protocol for effective treatment of heterogeneous ovarian cancer.

Methods: An amphiphilic polymer coated magnetic iron oxide nanoparticle was conjugated with near infrared dye labeled HER2 affibody and chemotherapy drug cisplatin. The effects of the theranostic nanoparticle on targeted drug delivery, therapeutic efficacy, non-invasive magnetic resonance image (MRI)-guided therapy, and optical imaging detection of therapy resistant tumors were examined in an orthotopic human ovarian cancer xenograft model with highly heterogeneous levels of HER2 expression.

Results: We found that systemic delivery of HER2-targeted magnetic iron oxide nanoparticles carrying cisplatin significantly inhibited the growth of primary tumor and peritoneal and lung metastases in the ovarian cancer xenograft model in nude mice. Differential delivery of theranostic nanoparticles into individual tumors with heterogeneous levels of HER2 expression and various responses to therapy were detectable by MRI. We further found a stronger therapeutic response in metastatic tumors compared to primary tumors, likely due to a higher level of HER2 expression and a larger number of proliferating cells in metastatic tumor cells. Relatively long-time retention of iron oxide nanoparticles in tumor tissues allowed interrogating the relationship between nanoparticle drug delivery and the presence of resistant residual tumors by *in vivo* molecular imaging and histological analysis of the tumor tissues. Following therapy, most of the remaining tumors were small, primary tumors that had low levels of HER2 expression and nanoparticle drug accumulation, thereby explaining their lack of therapeutic response. However, a few residual tumors had HER2-expressing tumor cells and detectable nanoparticle drug delivery but failed to respond, suggesting additional intrinsic resistant mechanisms. Nanoparticle retention in the small residual tumors, nevertheless, produced optical signals for detection by spectroscopic imaging.

Conclusion: The inability to completely excise peritoneal metastatic tumors by debulking surgery as well as resistance to chemotherapy are the major clinical challenges for ovarian cancer treatment. This targeted cancer therapy has the potential for the development of effective treatment for metastatic ovarian cancer.

Key words: targeted drug delivery, theranostic nanoparticles, resistant mechanism, MR image-guided cancer therapy, spectroscopic imaging

Introduction

Targeted cancer therapy utilizing surface receptors that are highly expressed on tumor cells has been used to treat human cancer. Antibodies or antibody-drug conjugates targeting cell receptors, such as HER2 (human epidermal growth factor receptor 2) and insulin-like growth factor receptor, have demonstrated therapeutic efficacy in cancer patients [1-3]. For example, anti-HER2 monoclonal antibodies have been used as the first-line therapy for HER2-positive (HER2+) breast cancer patients [4-6]. Despite clinical success in targeted cancer therapy, there is a wide range of therapeutic responses among cancer patients. Patients with drug-resistant residual tumors following treatment have a high incidence of tumor recurrence and an overall poor prognosis. It is well known that the levels of biomarker expression are highly heterogeneous among tumors from different patients and within tumors in the same patient [7, 8]. Histological definition of HER2+ tumors is based on over 10% of tumor cells having immunohistochemical staining intensity greater than 3+ or 2+ with *in situ* hybridization showing *HER2* gene amplification [9]. Therefore, patients classified as HER2+ in fact have a large fraction of tumor cells with a low level of HER2 expression. Although HER2-expressing tumor cells are detected in 10 to 20% of human ovarian cancer tissues, results of clinical trials using HER2 antibody targeted therapy have shown poor to modest therapeutic responses [10, 11]. The overall level of HER2 expression in ovarian cancer was found to be weaker and more heterogeneous than that of HER2+ breast cancer [8, 10]. Therefore, more effective combination therapies are necessary to treat ovarian cancers with highly heterogeneous tumor cells.

Chemotherapy drugs, such as platinum and taxol, have been widely used for the treatment of many solid cancers, including ovarian cancer [12, 13]. Although about 80% of ovarian cancer patients showed initial response to chemotherapy following cytoreductive surgery, most of them developed recurrent tumors that were resistant to cisplatin within 18 to 24 months [14]. The failure of chemotherapy is predominantly due to systemic toxicity of the drug that limits drug dose, in addition to intrinsic and acquired drug resistance in a subpopulation of tumor cells [12].

Nanoparticle drug carriers have the potential to selectively deliver chemotherapy drugs into tumors, thereby overcoming drug resistance while reducing systemic toxicity. Increasing evidence shows that biomarker-targeted therapy and nanoparticle drugs have improved delivery into tumors, leading to enhanced therapeutic responses [15-19]. The effect of nanoparticle drug carriers has been shown in mouse ovarian tumor models [15, 18-21]. Although currently FDA-approved nanoparticle drugs are based on non-targeted liposomes, polymeric nanoparticles, and human serum albumin formulations, various targeted and multifunctional nanoparticle drug carriers have been developed and their effects have been demonstrated in mouse tumor models and clinical trials [16, 22].

Theranostic nanoparticles with the ability to both deliver drug and image tumors are a promising platform for the development of image-guided cancer therapy of heterogeneous and drug-resistant human cancers [23-26]. Our previous studies showed targeted delivery and imaging in an orthotopic human ovarian cancer model using HER2-targeted multimodal nanoparticle imaging probes consisted of a near-infrared (NIR) 830 dye-labeled HER2 affibody ($Z_{HER2:342}$) conjugated to magnetic iron oxide nanoparticles (NIR-830-$Z_{HER2:342}$-IONP) [27]. For this study, we developed HER2-targeted theranostic nanoparticles carrying cisplatin (NIR-830-$Z_{HER2:342}$-IONP-Cisplatin) with combined optical, MRI, and spectroscopic imaging capacity. The unique properties of this theranostic nanoparticle platform provide a means to investigate several important questions concerning targeted delivery and intratumoral distribution in heterogeneous HER2-expressing human tumors. This can be especially useful for tumors with differential levels of cell receptors and can ultimately determine whether poor drug delivery is one of the causes of tumor resistance to targeted therapy. Non-invasive MRI was used for monitoring nanoparticle drug delivery in the primary tumor and individual metastatic lesions. The feasibility and sensitivity of intraoperative imaging of resistant tumors following targeted therapy were also determined. Results of those studies should provide a strong rationale and supportive evidence for the development of a new theranostic nanoparticle-based cancer therapy protocol for effective treatment of human ovarian cancer with highly heterogeneous HER2 expression and resistance to therapy.

Methods

Production of NIR-830-$Z_{HER2:342}$-IONP-Cisplatin nanoparticles

HER2 affibody ($Z_{HER2:342\text{-}Cys}$) was produced from a bacterial-expressing system using an established protocol [28]. $Z_{HER2:342\text{-}Cys}$ was labeled with NIR-830-maleimide dye that was synthesized from IR-783 dye in our group [29]. Ten NIR-830-HER2 affibody molecules were conjugated to each

amphiphilic polymer-coated magnetic iron oxide nanoparticle (IONP, 10 nm core size, Ocean Nanotech, LLC, San Diego, CA, USA) via an amide bond mediated by ethyl-3-dimethyl amino propyl-carbodiimide and sulfo-N-hydroxysuccinimide. Cisplatin (Polymed Therapeutics Inc, Houston, TX, USA) was conjugated to NIR-830-$Z_{HER2:342}$-IONP by mixing freshly dissolved cisplatin solution (10 mg/mL in 10 mM borate buffer, pH 6.2) with NIR-830-$Z_{HER2:342}$-IONP at a ratio of 1 mg of iron equivalent of IONPs with 1 mg of cisplatin for 4 h at room temperature. Cisplatin was conjugated to IONPs by the formation of a coordinate bond between platinum (Pt+) and carboxylate group (O=C-O-, Lewis base) on the polymer surface of IONP. Unconjugated cisplatin was separated from nanoparticle conjugated cisplatin by centrifuging through a Nanosep 100kDa molecular weight cut-off filter column (Pall Corp., MI, USA). The hydrodynamic size and zeta-potential of the nanoparticles were determined using a Zetasizer Nano-ZS (Malvern Instruments, Southborough, MA, USA). *In vitro* drug release was examined in phosphate-buffered saline (PBS) at pH 5 or pH 7.5 and under rotation at 37 °C in a Nanosep 3kDa cut-off filter column (Pall Corp.). The amount of released cisplatin was determined using a modified platinum colorimetric assay that was based on the reaction of platinum with o-phenylenediamine [30].

Orthotopic human ovarian cancer xenograft model

A firefly luciferase gene stably transfected human SKOV3 ovarian cancer cell line (SKOV3-Luc) was provided by Dr. Daniela Matei at Indiana University-Purdue University. Cells were cultured in McCoy's 5A supplemented with 10% fetal bovine serum and 1% penicillin and streptomycin. Orthotopic xenograft model was established by injecting 5 x 10^4 cells in 15 µL of PBS into the ovary bursa of female athymic nude mice (6- to 8-week-old, Harlan laboratories, Indianapolis, IN, USA) using an Emory Institutional Animal Care and Use Committee approved protocol.

Prussian blue staining

To determine target specificity in cells, 100 nM of NIR-830-$Z_{HER2:342}$-IONP-Cisplatin or non-targeted IONPs were added to cultured cells for 2-3 h. After removing the culture medium, cells were washed and fixed with 4% paraformaldehyde in PBS for 20 min. Prussian blue solution prepared by 1:1 mixture of 10% potassium ferrocyanide (Sigma-Aldrich, St. Louis, MO, USA) and 20% HCl acid was added for 30 min to 2 h at 37 ºC. To determine IONP delivery in tumors, frozen tumor tissue sections were incubated with the aforementioned staining solution for 3 h and then counter-stained with a nuclear fast red solution (Sigma-Aldrich).

Non-invasive imaging of targeted delivery of nanoparticle in ovarian cancer and detection of drug-resistant tumors

Bioluminescence imaging (BLI): The growth of SKOV3-luc tumors was monitored using a BLI system following an i.p. injection of D-luciferin substrate (IVIS Spectrum *in vivo* imaging system, Perkin Elmer, Waltham, MA, USA).

NIR optical imaging: Optical imaging was conducted using the Kodak *In Vivo* FX imaging system (Carestream Health Inc, Rochester, NY, USA). All optical images were captured using an 800-nm excitation and 850-nm emission filter set and analyzed using Kodak imaging software.

MRI: A clinical, 3-Tesla (3-T) MRI scanner (Siemens Medical System, Tarrytown, NY, USA) with a customized coil or animal 4.7-T MRI scanner (Oxford Magnet Technology, Oxford, UK) was used for murine imaging. T_2-weighted fast spin-echo imaging sequence with a repetition time (TR) of 5000 millisecond (ms), echo time (TE) of 28 ms, field-of-view (FOV) of 40 × 70 mm, and slice thickness of 1 mm was used to acquire multiple slices of axial MR images for each animal on the 4.7-T MRI scanner. On the 3-T MRI scanner, T_2-weighted turbo spin-echo imaging sequence was performed with the following imaging parameters: turbo factor = 14, TR = 5000 ms, TE = 65 ms, image matrix = 60 × 256, FOV = 28 × 120 mm^2, slice thickness = 1.5 mm for coronal MR images. Signal intensity of T_2-weighted spin-echo images in the tumor following the administration of nanoparticles was quantitatively analyzed in all MR image slices of all identifiable tumor areas, including primary and metastatic sites. Averaged signal intensities of the regions of interest (ROIs) of tumor areas were selected for measuring IONP-induced MRI T_2 signal change using ImageJ software (National Institutes of Health, Bethesda, MD, USA). Signal intensity of T_2-weighted MR images in a selected muscle area was measured for each mouse and each MRI scan to serve as an internal control. The relative signal intensity of T_2-weighted MRI of the tumor area in each MR image was calculated as the ratio of signal intensities of T_2-weighted MRI in tumor area to that in normal muscle.

Evaluation of efficacy of targeted therapy in the orthotopic ovarian cancer xenograft model

Three weeks after the tumor cell implantation,

nude mice bearing orthotopic SKOV3 ovarian tumors were randomized to different treatment groups. Tumor growth was confirmed by BLI. Mice were subjected to therapeutic interventions, twice per week for three weeks with a total of six tail vein injections. Mice were sacrificed five days after the last treatment, and tumor and normal tissues were collected for histological analysis.

Immunohistochemical and immunofluorescence analyses

The level of HER2 expression was determined by either immunohistochemical analysis or immunofluorescence labeling on frozen or paraffin-embedded tumor tissue sections using an anti-HER2 antibody (cat # 2242, Cell Signaling, Danvers, MA, USA) at 1:100 dilution and standard immunostaining protocols. Secondary antibodies conjugated to *horseradish peroxidase* (HRP, immunohistochemical) or Alexa fluor-488 (immunofluorescence) were used. HRP was detected with a 3,3'-diaminobenzidine substrate. To determine proliferating cells, an anti-Ki67 antibody (Clone 7B11, Invitrogen, Carlsbad, CA, USA) was used to label the tissue section. Alexa Fluor-555 labeled secondary antibody was used for immunofluorescence imaging. Mouse anti-human CK19 antibody (C-6930, Sigma-Aldrich) was used to identify ovarian cancer cells. Rat anti-mouse CD68 monoclonal antibody (MCA1957, BioRad Laboratories, Inc., Hercules, CA, USA) was used to label macrophages. For immunofluorescence, slides were counter-stained with Hoechst 33342 (Thermo Fisher Scientific, Waltham, MA, USA).

Detection of drug-resistant tumors using spectroscopic imaging

A custom-built, handheld spectroscopic imaging device was used for this study [31]. Signals of spectroscopic and NIR imaging were detected using a pen-like probe and then processed using a custom software [31]. The processed imaging signals were co-displayed with the imaged field captured by a CCD camera on a color monitor. Five days following the last treatment, tumor-bearing mice were sacrificed and then subjected to spectroscopic imaging of drug-resistant tumors and normal tissues. The spectroscopic signal intensity was recorded for each detection.

Statistical analysis

Data are presented as mean ± standard deviation, and all experiments were performed in at least triplicates. Statistically significant differences ($p \leq 0.05$) between groups with respect to tumor weights were determined using the standard Student's *t*-test.

Results

Establishment of an orthotopic and metastatic human ovarian cancer xenograft model with tumor developmental stages and heterogeneous levels of HER2 expression that resemble human ovarian cancer

Effective treatment of heterogeneous tumors using receptor-targeted therapy in human cancer patients will require a combination of: (**i**) assessment of targeted receptor expression by molecular imaging, (**ii**) noninvasive imaging for monitoring targeted drug delivery and therapeutic response, and (**iii**) image-guided surgery for the removal of drug-resistant residual tumors (**Figure 1A**). Most previous studies used mouse tumor models bearing single subcutaneous or orthotopic tumor, which could not provide information on the correlation between heterogeneous levels of biomarker expression with targeted delivery of nanoparticle drug carriers and molecular imaging signals in individual primary and metastatic tumors. To determine the ability of HER2 targeted theranostic nanoparticles in targeted delivery and non-invasive imaging of human tumors with highly heterogeneous HER2 expression, we established and characterized an orthotopic human ovarian cancer xenograft model that recapitulated developmental stages and heterogeneous HER2 expression in human ovarian cancer (**Figure 1B-C**). Noninvasive BLI and gross examination of the peritoneal cavity of mice demonstrated that tumor growth and metastatic spreading correlated with disease progression in ovarian cancer patients. H&E staining of tumor tissues showed the initial primary tumor inside the ovary (stage I), metastatic tumors developed in the peritoneal cavity (stage III), and then in distant organs, such as the lung (stage IV) (**Figure 1B**). Differential expression levels of HER2 in the tumors were found among the primary tumor and metastatic lesions collected from the peritoneal cavity. Double labeling immunofluorescence further showed that metastatic tumors had high levels of HER2 expression and proliferating cells (Ki67 positive) than that of the primary tumor (**Figure 1C**). Therefore, this mouse tumor model should allow for the evaluation of the effect of HER2-targeted therapy using theranostic nanoparticles, the efficiency of targeted delivery of nanoparticle drug carriers, and the differential therapeutic effects on different tumors in the same mice using non-invasive MRI, optical imaging, and histological analysis.

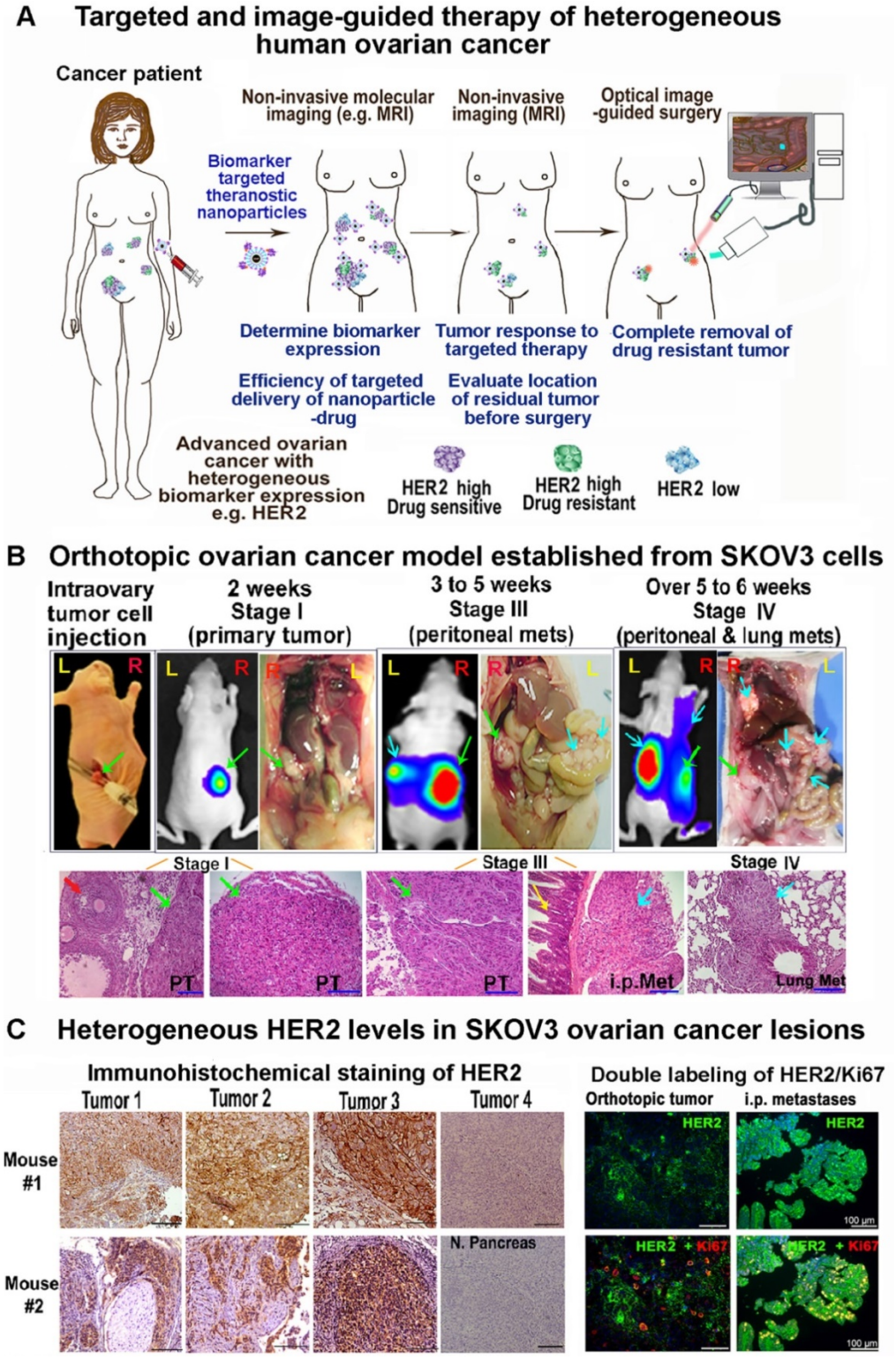

Figure 1. Development of an integrated protocol of targeted drug delivery and image-guided therapy. (A) Schematic illustration of targeted and image-guided therapy of advanced ovarian cancer with heterogeneous HER2 expression using theranostic nanoparticles. Systemic delivery of HER2 targeted theranostic nanoparticles leads to drug accumulation in HER2-expressing ovarian tumors. MRI can be used to evaluate nanoparticle drug delivery in individual tumors with different levels of HER2 in the peritoneal cavity. It can also assesse therapeutic response in tumors. Residual tumors, due to a low level of HER2 or intrinsic drug resistance, produce NIR signals for detection and removal by image-guided surgery. **(B)** Orthotopic ovarian cancer xenograft model derived from HER2+ human ovarian cancer SKOV3-luc cell line was established by direct injection of cells into the ovary of nude mice. Growth and staging of the tumor could be identified by BLI. Bright-field images were included for visualizing tumor locations. H&E-stained tissue sections showed stage I tumor in the ovary (PT, green arrow), stage III with i.p. metastases (blue arrows), and stage IV with lung metastases. Red arrow: normal follicle. Yellow arrow: intestine. **(C)** Immunohistochemical staining of tumor tissue sections collected from two representative mice using an anti-HER2 antibody. The levels of HER2 expression from negative to strongly positive were detected in four tumors in Mouse #1 and three tumors in Mouse #2. Normal pancreas: a negative control for HER2 labeling. Dual immunofluorescence labeling of HER2 (green) and Ki67 (red) of primary and metastatic tumors showed metastatic tumors had a higher level of HER2 and more proliferating cells (red) than primary tumors. Blue: Hoechst 33342 nuclear staining. Scale bars: 100 μm.

Characterization of HER2-targeted theranostic nanoparticles *in vitro* and *in vivo*

HER2-targeted IONP conjugated with cisplatin was prepared in two steps as shown in **Figure 2A**. Chemical analysis of platinum (Pt) content showed that about 0.5 mg of cisplatin was conjugated to 1 mg of iron equivalent IONPs. Electron microscopy images showed uniformly sized magnetic IONPs with a 10 nm core (**Figure 2B**). Dynamic light scattering measurement determined that the hydrodynamic diameters for non-targeted IONP, IONP-Cisplatin, NIR-830-$Z_{HER2:342}$-IONP and NIR-830-$Z_{HER2:342}$-IONP-Cisplatin were 15.3, 19.2, 21.5, and 23.6 nm respectively (**Figure 2C**). Zeta potentials of the nanoparticles were -46.2 millivolts (mV) (IONP), -34.9 mV (NIR-830-$Z_{HER2:342}$-IONP), -31.7 mV (NIR-830-$Z_{HER2:342}$-IONP-Cisplatin), and -33.6 mV (IONP-Cisplatin). Under pH 7.5 in PBS for 18 h, about 25% of conjugated cisplatin was released. However, under pH 5, drug-release rate reached 80% at 18 h, suggesting a pH-dependent drug release (**Figure 2D**). Target specificity of NIR-830-$Z_{HER2:342}$-IONP-Cisplatin was determined in the HER2+ human ovarian cancer SKOV3 cells *in vitro*. Accumulation of HER2-targeted IONPs in tumor cells was demonstrated by Prussian blue staining (**Figure 2E**). Furthermore, a stronger cytotoxic effect was observed in high HER2-expressing SKOV3 cells relative to low HER2-expressing OVCAR3 cells (**Figure S1**).

Targeted delivery of NIR-830-$Z_{HER2:342}$-IONPs in ovarian cancer xenografts following intravenous (i.v.) injection was determined by optical imaging. Forty-eight hours following i.v. injection of NIR-830-$Z_{HER2:342}$-IONPs into tumor bearing mice, strong optical signals were detected in both primary tumor in the ovary and metastatic lesions in the lung and peritoneum (**Figure 2F** and **Figure S2**). Control mice that received non-targeted NIR-830-bovine serum albumin (BSA)-IONPs had weak optical signals in primary and peritoneal metastatic tumors (**Figure 2F**). *Ex vivo* optical imaging showed that signal intensity was 1.6- and 2.6-fold higher in the primary tumor and lung metastases in the mice that received NIR-830-$Z_{HER2:342}$-IONPs than those treated with non-targeted NIR-830-BSA-IONPs (**Figure 2F**). Chemical analysis of IONP in tumors showed a 7-fold higher iron concentration in the tumors treated with the targeted IONPs compared to non-targeted IONPs (**Figure 2F and Figure S2**). Histological and chemical analysis of tumor tissues further confirmed the accumulation of targeted IONPs in primary tumors and lung metastases with 13% of total delivered NIR-830-$Z_{HER2:342}$-IONPs found in tumor (**Figure S2**).

Magnetic IONPs have been used for the development of MRI contrast agents and theranostic IONPs [32-34]. Accumulation of IONPs primarily shortens the transverse relaxation times, i.e. T_2 and T_2*, which lead to prominent signal decrease or "negative contrast" of targeted tissue in T_2-weighted MRI. To assess the functionality of NIR-830-$Z_{HER2:342}$-IONPs as a superparamagnetic MRI contrast agent for imaging intratumoral delivery of theranostic IONPs, mice were subjected to MRI before and after the delivery of the nanoparticles. T_2-weighted MRI of the mouse treated with NIR-830-$Z_{HER2:342}$-IONPs showed a 31.9% of the relative signal reduction of T_2-weighted spin-echo image in tumors, indicating targeted delivery of the nanoparticles (**Figure 2G**).

Significant inhibition of tumor growth following targeted therapy

We further investigated the therapeutic efficacy of HER2-targeted therapy using NIR-830-$Z_{HER2:342}$-IONP-Cisplatin. Tumor-bearing nude mice received 5 mg/kg cisplatin-equivalent dose of NIR-830-$Z_{HER2:342}$-IONP-Cisplatin, cisplatin, or non-targeted IONP-Cisplatin, twice per week for a total of six treatments. Five days after the last injection, no-treatment control mice displayed large primary tumors and peritoneal metastases (**Figure 3A-C**). However, treatment with NIR-830-$Z_{HER2:342}$-IONP-Cisplatin significantly inhibited the growth of both primary and peritoneal metastatic tumors, and in two of six mice, led to complete tumor regression (**Figure 3A-C**). Results of our *in vivo* study showed that systemic delivery of HER2-targeted IONPs carrying cisplatin at 5 mg/kg dose had stronger tumor growth inhibition on peritoneal metastases than primary tumors (**Figure 3A-C**). The majority of mice that received HER2-targeted IONP-Cisplatin had very small primary tumors and no-visible peritoneal metastases. Furthermore, even after treatments with a very low dose of 0.5 mg/kg of cisplatin equivalent of NIR-830-$Z_{HER2:342}$-IONP-Cisplatin, the mice had marked inhibition of i.p. metastases while having a modest response in primary tumors (**Figure S3**).

Overall, treatment with NIR-830-$Z_{HER2:342}$-IONP-Cisplatin led to 88% of growth inhibition of the total tumor volumes, including all visible primary and metastatic tumors in the peritoneal cavity, compared to those of no treatment control mice (**Figure 3A**). Treatment with non-targeted IONP-Cisplatin resulted in 45% of tumor growth inhibition. The same dose of conventional cisplatin led to 66% inhibition of tumor growth. Statistical analysis using student's *t*-test showed that the anti-tumor growth effect of the targeted-IONP-Cisplatin was highly significant compared to no-treatment control ($p<0.005$), and significant compared to cisplatin ($p<0.05$) and non-targeted IONP-Cisplatin ($p<0.01$) treated mouse

groups. Although the mouse groups treated with cisplatin or non-targeted IONP-Cisplatin had reduced volumes of primary tumors and small peritoneal tumors, only cisplatin treatment mouse group showed statistically significant inhibition compared to the no-treatment control group ($p \leq 0.01$).

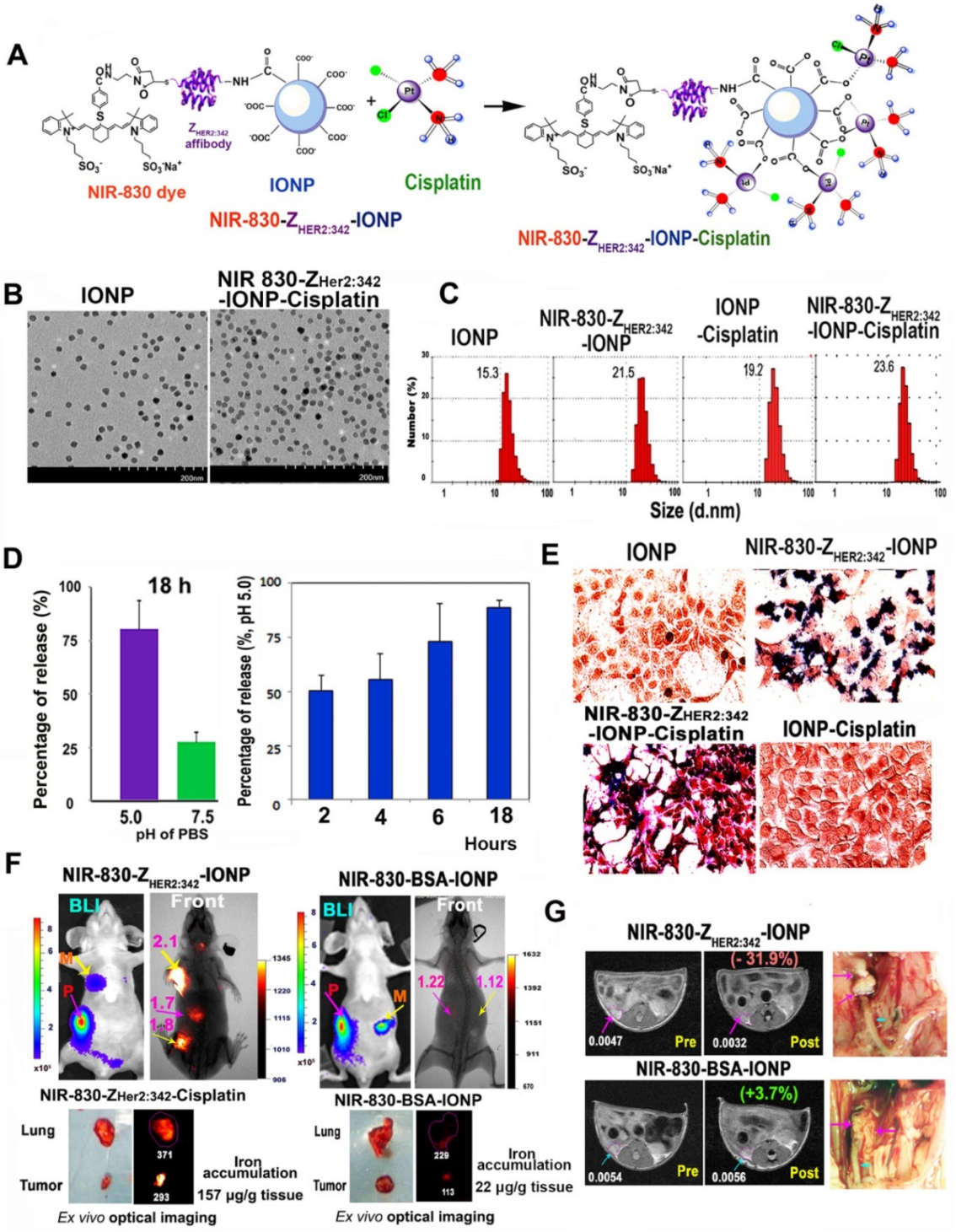

Figure 2. Characterization of HER2-targeted theranostic nanoparticle carrying cisplatin. (A) Production of HER2-targeted theranostic nanoparticle, NIR-830-$Z_{HER2:342}$-IONP-Cisplatin. **(B)** Electron microscopy images of different IONPs. **(C)** Dynamic light scattering analysis of nanoparticle sizes. **(D)** Platinum-loaded, HER2 targeted IONPs showed faster drug release in pH 5.0 buffer than that under pH 7.5. Percentage of drug release was calculated from the initial drug content of NIR-830-$Z_{HER2:342}$-IONP-Cisplatin. **(E)** *In vitro* target specificity detected by Prussian blue staining. **(F)** *In vivo* targeted delivery. Optical imaging at 48 h following the second i.v. injection of 400 picomolar (pmol) of NIR-830-$Z_{HER2:342}$–IONP. Primary tumor (pink arrow) and metastatic lesions in the peritoneal cavity and lung (yellow arrows). Imaging results performed after the first injection is shown in **Figure S2**. There was no bright optical signal in the mice received non-targeted NIR-830-BSA-IONP. Locations of tumors were identified by bioluminescence imaging (BLI). Pink numbers: ratio of optical signal in tumor and body background. *Ex vivo* imaging confirmed stronger optical signal in primary tumor and lung metastases in targeted IONP treated mice than those treated with non-targeted IONPs. Chemical analysis of iron concentrations in the primary tumors are shown. **(G)** T_2-weighted MRI performed Pre and 24-h post i.v. delivery of NIR-830-$Z_{HER2:342}$–IONP showed a signal intensity decrease of T_2-weighted MRI in the primary tumor (~5 mm in diameter) (pink arrows). No T_2 signal intensity decrease was seen in the tumor of the mice that received non-targeted NIR-830-BSA-IONP. White numbers: the mean relative signal intensity in tumors. Bright field images of the peritoneal cavity showed primary tumors in the ovary (pink arrows). Blue arrow: fallopian tube.

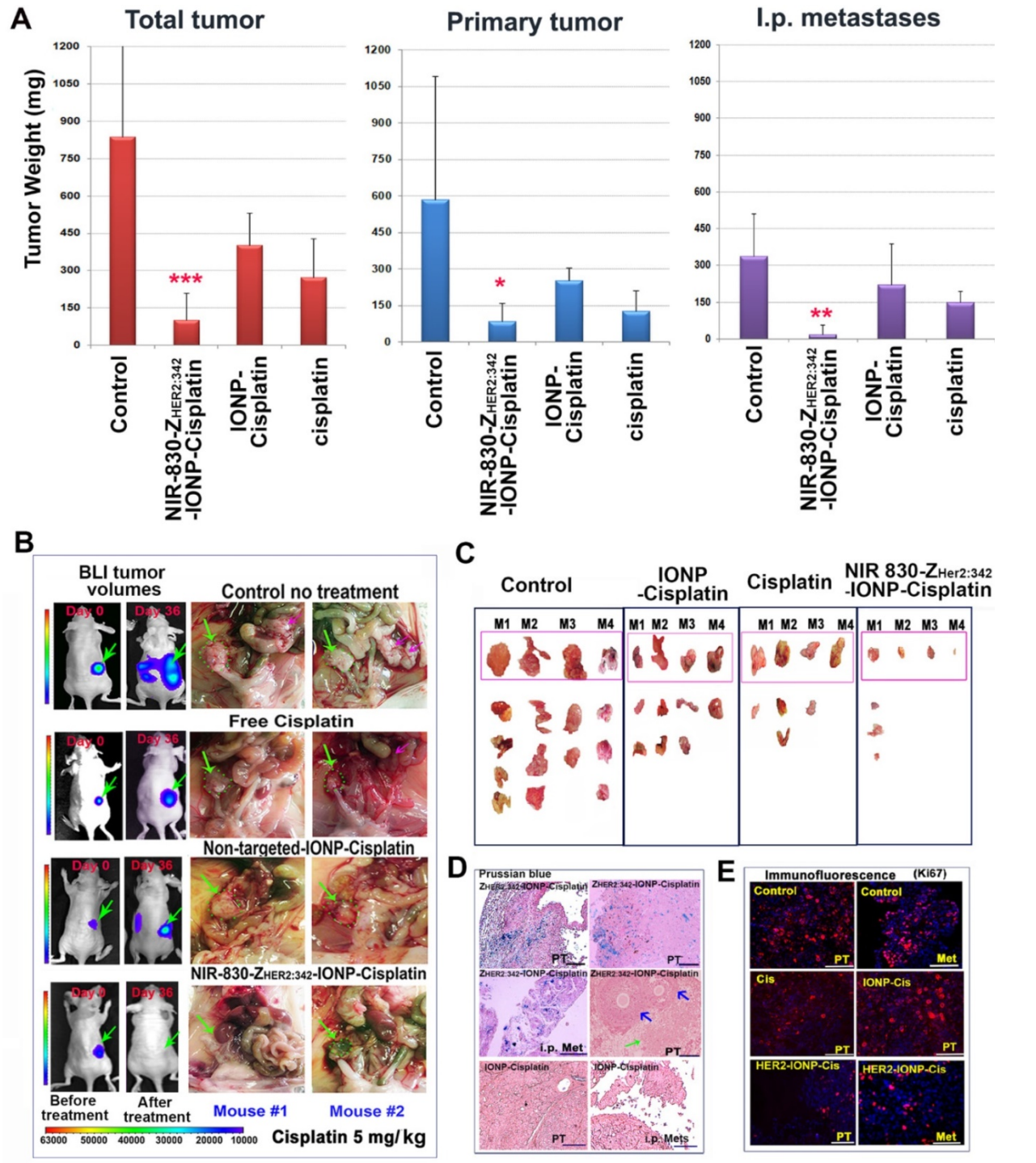

Figure 3. Therapeutic effect of HER2-targeted IONP-Cisplatin on primary and metastatic ovarian tumors. (A) Tumor weights of primary and metastatic tumors following 5 mg/kg of cisplatin dose twice per week for a total of six treatments. The mean tumor weights of total visible tumors collected from the peritoneal cavity, primary tumor, and i.p. metastatic tumors (Mets) are shown. (n = 6-8 mice/ control, cisplatin and targeted IONP groups; n = 3 mice/IONP-Cisplatin). Student's *t*-test: No treatment vs. targeted IONP-Cisplatin: total tumor: p=0.004, Primary tumor: p=0.026, Mets: p=0.006. Targeted-IONP-Cisplatin vs cisplatin: total tumor: p=0.02. Primary tumor: p=0.035, Mets: p=0.005. **(B)** Therapeutic responses in two representative mice shown as BLI images and bright-field pictures that identified tumors in the peritoneal cavity. Green arrows: primary tumors. Pink arrows: i.p. metastases. **(C)** *Ex vivo* pictures of tumors collected from mouse groups. Primary tumor: top pink boxed. Multiple i.p. metastases from mouse groups are shown (n = 4 mice/group). Three of four mice treated with targeted IONP-Cisplatin lack visible i.p. metastases. **(D)** Prussian blue staining of tumor tissue sections showed the presence of IONP in primary tumor (PT) and i.p. metastases (Mets) in targeted IONP-Cisplatin treated mice. Some residual primary tumor areas (green arrow) and adjacent normal follicle (blue arrows) lacked IONP positive cells. Non-targeted IONP-Cisplatin treated tumors showed a very low level of IONP positive cells. **(E)** Immunofluorescence labeling of cell proliferation marker Ki67. A low level of Ki67 positive cells (red) was found in the primary and metastatic tumors treated with NIR-830-$Z_{HER2:342}$-IONP-Cisplatin (HER2-IONP-Cis). Blue: Hoechst 33342 nuclear staining. Scale bar: 100 μm.

Histological analysis of tumor tissues showed intratumoral necrotic areas in NIR-830-$Z_{HER2:342}$-IONP-Cisplatin treated tumors. However, dense tumor cells were found in the no-treatment control, cisplatin and IONP-Cisplatin treated tumors (**Figure S4**). Prussian blue staining revealed high levels of

IONPs in tumor tissues treated with NIR-830-$Z_{HER2:342}$-IONP-Cisplatin. It seemed that normal follicles in the ovary lacked accumulation of IONPs (**Figure 3D**). IONPs were not detected in the primary and metastatic tumor tissues obtained from mice that received non-targeted IONP-Cisplatin (**Figure 3D**). Furthermore, immunofluorescence labeling showed that the residual tumors treated with NIR-830-$Z_{HER2:342}$-IONP-Cisplatin had a markedly lower level of Ki67-positive proliferating cells in the primary and metastatic tumors (~1.6%) than that of no-treatment control (31%). There was a statistically significant difference between the two groups (p = 0.009, n = 5 image fields) (**Figure 3E**).

An advantage of nanoparticle-based drug carriers is the reduction of systemic toxicity since they are unable to pass through normal vessels to be delivered into normal tissues, with the exception of macrophages in the liver and spleen [35]. In our study, there was no apparent systemic toxicity observed in mice treated with NIR-830-$Z_{HER2:342}$-IONP-Cisplatin. Serological examination and histological analysis showed that there was no damage in the liver and kidney (**Figures S5-S6**). However, mice treated with 5 mg/kg of unconjugated cisplatin showed noticeable tissue damage in normal organs (**Figure S6**).

MRI detection of differential tumor responses to the targeted therapy in mice bearing orthotopic ovarian tumors

We further examined the ability of monitoring drug delivery and therapeutic response in ovarian tumors using MRI. Following six treatments, BLI revealed marked decreases in the tumor volumes of mice treated with NIR-830-$Z_{HER2:342}$-IONP-Cisplatin (5 mg/kg) compared with untreated or NIR-830-$Z_{HER2:342}$-IONP (no drug) treated mice (**Figure 4A**). However, differential signal intensities of T_2-weighted MRI were found in residual tumors following NIR-830-$Z_{HER2:342}$-IONP-Cisplatin treatment. In comparison with tumor size and T_2 signal intensity detected in the control mouse, a good responder mouse M2 had a much smaller residual tumor with 28% of signal intensity decrease in T_2-weighted MRI, while mouse M1 showed an intermediate-sized residual tumor without a T_2 signal intensity decrease, suggesting lack of IONP accumulation in this portion of the residual tumor (**Figure 4A**). Our results also showed that HER2-targeted delivery played a key role for the observed changes in the signal intensity of T_2-weighted MRI and therapeutic effect since systemic delivery of non-targeted IONP or IONP-Cisplatin did not show a T_2 signal intensity decrease in tumors (**Figure S7**).

Next, we examined whether MRI could monitor response to therapy in primary and metastatic tumors. T_2-weighted spin echo MRI was performed on mice following the fifth and sixth therapy. Comparison of two MR images of the untreated control mice showed continued growth of the primary and metastatic tumors with a high level of T_2 signal intensity (**Figure 4B**). In the mouse M3 that had an intermediate therapeutic response, the first MR image detected a smaller primary tumor with a 13.8% T_2 signal intensity decrease but no visible metastases (**Figure 4B**). In the second MR image, an enlarged primary tumor without a T_2 signal intensity decrease was detected (**Figure 4B**). However, a good responder mouse M4 had a very small primary tumor with a 50.5% T_2 signal intensity decrease in the first MRI. Following an additional treatment, there was no detectable tumor in the original tumor site in the second MRI (**Figure 4B**). Although a very weak BLI signal could still be detected in the primary tumor area, there was no visible tumor mass in the ovarian area of the peritoneal cavity (**Figure 4B**). In contrast, the mouse treated with IONP-Cisplatin did not show T_2 signal intensity change and had slightly reduced primary tumor and detectable metastases in the first MRI (**Figure 4B**). Prussian blue staining showed a high level of IONPs in the tumor tissues of the mice treated with NIR-830-$Z_{HER2:342}$-IONP or NIR-830-$Z_{HER2:342}$-IONP-Cisplatin (**Figure 4C**). Therefore, our results supported the feasibility of using MRI to monitor therapeutic response in individual tumors in the same or different mice following targeted therapy using theranostic IONPs.

Since macrophages in tumor tissues could take-up nanoparticles non-specifically, double immunofluorescence labeling was performed to confirm targeted delivery of NIR-830-$Z_{HER2:342}$-IONP-Cisplatin into ovarian tumor cells. Frozen tumor tissue sections obtained from the mice treated with the targeted IONP-Cisplatin were doubly labeled with an anti-CK 19 antibody (tumor cells) and an anti-CD68 antibody (macrophages). Under a fluorescence microscope equipped with NIR fluorescence filter, we detected a high level of NIR signals produced from the nanoparticles in tumor tissue sections. Most NIR-signal-positive cells co-localized with CK19-positive tumor cells. CD68-positive macrophages were found near CD19-positive tumor cells and some of them have NIR-positive nanoparticle signals. Macrophages without NIR signal were also detected in the tumor. Thus, despite the possibility of non-specific uptake of the nanoparticle drug in tumors by macrophages, our result showed that a high level of the targeted IONP-Cisplatin was taken up by tumor cells.

However, macrophages in tumor tissues could also engulf tumor cell debris with the nanoparticles. Although those macrophages could be identified by histological analysis, this factor should be taken into consideration when the IONP-positive cells were used as an indication for the possible cause of therapy resistance.

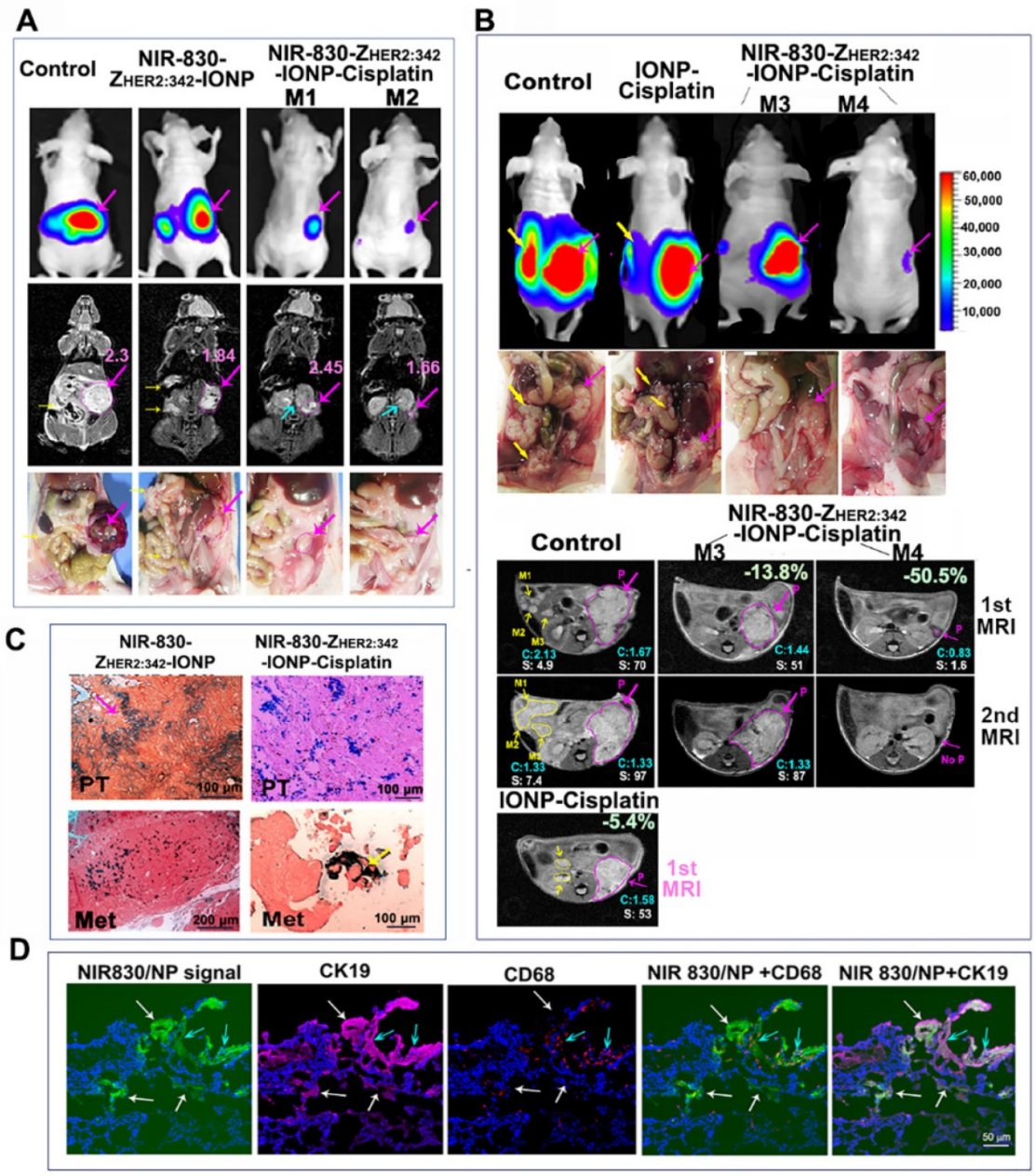

Figure 4. Non-invasive MRI detection of response to targeted therapy following systemic delivery of HER2-targeted theranostic IONP-Cisplatin. (A) T_2-weighted MRI. Two days following the sixth therapy, BLI and coronal MR images showed tumor sizes and MRI contrasts in good responder (M2), intermediate responder (M1), no-treatment and targeted IONP (no drug) control mice. Mouse M2 had a smaller tumor and lower T_2 signal intensity than those in mouse M1, suggesting a higher level of theranostic IONP accumulation in mouse M2 that led to a better response. **(B)** Transverse MR images. No-treatment control mouse following the fifth treatment (1st MRI) had a large primary tumor and several large metastases with a high T_2 signal intensity. Good responder (M4) had a very small primary tumor with a decreased T_2 signal intensity. The intermediate responder (M3) had a primary tumor with a 13.8% T_2 signal intensity reduction compared with no treatment control. Both mice had no visible i.p. metastases. IONP-Cisplatin treated tumor had an intermediate size primary tumor and detectable i.p. metastases with a high T_2 signal intensity. The second MRI after sixth treatment revealed progressive growth of primary and metastatic tumors in the control mice. A small tumor in the good responder mouse M4 became invisible on the MR image. The primary tumor in mouse M3 continued to grow and did not show a decrease in T_2 signal intensity. Pink arrows and line-circled areas: primary tumor. Yellow arrows: i.p. metastatic tumors; blue arrow: kidney. P: primary tumor. M_{1-3}: selected i.p. metastases for quantification. Numbers in blue color C: the mean value of T_2 signal intensity of identifiable tumor areas in all MR image slices. Number shown as white S: quantification of the tumor areas of the primary and selected i.p. metastases in pixel in one representative MRI slice as shown. **(C)** Prussian blue staining in primary (PT) and i.p. metastatic (Met) tumor tissue sections. **(D)** Double immunofluorescence labeling to identify tumor cells (CK19, purple), and macrophage (CD68, red). NIR signal of nanoparticles (green). Blue fluorescence: Hoechst 33342. White arrows: IONPs in tumor cells. Blue arrows: IONPs in macrophages.

Optical imaging of drug-resistant tumors and mechanisms of heterogeneous therapeutic responses in tumors

The ability of optical imaging of accumulation of theranostic nanoparticles in tumors made it possible to examine targeted delivery of nanoparticle drugs as well as the presence of drug-resistant tumors. First, we analyzed optical signals from two representative mice that were treated with NIR-830-$Z_{HER2:342}$-IONP-Cisplatin (5 mg/kg cisplatin) and showed a relatively poor (M2) or good (M3) therapeutic response among all mice in the targeted therapy group (**Figure 5A**). Mouse M1 received NIR-830-$Z_{HER2:342}$-IONP (no cisplatin) as a delivery control to assess the efficiency of targeted nanoparticle delivery in tumors after repeated systemic deliveries but without killing of tumor cells containing the nanoparticles. We detected much stronger optical signals in metastatic tumors than in the primary tumor, although the primary tumor was larger than peritoneal and lung metastatic tumors as shown in BLI (**Figure 5A**). Strong optical signals were the result of increased accumulation of the targeted nanoparticles in the growing tumors. Immunofluorescence labeling revealed that the primary tumor tissue has from weak-to-intermediate levels of HER2 expression while i.p. metastatic tumors had a much higher level of HER2 compared to the primary tumors (**Figure 5B**). We also detected a high level of IONP accumulation in metastatic tumor cells (**Figure 5B**).

As expected, BLI revealed markedly smaller peritoneal tumors in the mice after six systemic deliveries of NIR-830-$Z_{HER2:342}$-IONP-Cisplatin compared to the mice treated with the targeted nanoparticles without carrying cisplatin (**Figure 5A**). Heterogeneous optical signals were detected in the residual areas in the mice. For example, mouse M2 had a poorer therapeutic response with a relatively large primary tumor and was the only mouse with peritoneal metastases in the mouse group following the targeted therapy at 5 mg/kg cisplatin dose (**Figure 5A**). Noninvasive optical imaging showed an intermediate level of optical signal in the residual metastatic tumor but a weaker signal in the primary tumor. Prussian blue staining revealed that the primary tumor that survived the targeted therapy had a low level of IONP accumulation (**Figure 5B**). Immunofluorescence labeling of the residual tumor tissue sections showed that most of the resistant tumor cells in the primary tumor and a large portion of the metastatic tumor had a low level of HER2 expression, except a small subpopulation of cells on the edge of the metastatic tumor expressed HER2 (**Figure 5B**). Therefore, a low level of HER2 expression in a subpopulation of tumor cells was the major cause of inefficient delivery of theranostic IONPs in those tumor cells to effectively kill cells. However, immunofluorescence labeling using an anti-Ki67 antibody showed that the presence of a low level of NIR-830-$Z_{HER2:342}$-IONP-Cisplatin was still able to inhibit cell proliferation in the primary and metastatic residual tumors that led to an intermediate therapeutic response compared to no treatment control mouse group (**Figure 5C**). In a good responder mouse M3, a strong optical signal was detected in the area that had a low luciferase activity (**Figure 5A**). After sacrificing the mouse, there was no visible tumor in the ovary and peritoneal cavity. Histological analysis of collected ovarian tissue showed the presence of microscopic residual tumor with a few HER2-positive tumor cells at the edge and some Prussian blue positive residual tumor cells in the ovarian tissue (**Figure 5B**). There was no i.p. metastases in this mouse.

Since tumor response to chemotherapy drug is closely associated with the amount of the drug molecules delivered into tumors, we examined the therapeutic response when tumor-bearing mice received a lower dose of cisplatin equivalent of NIR-830-$Z_{HER2:342}$-IONP-Cisplatin. Although mice treated with a 2 mg/kg cisplatin dose of the targeted theranostic nanoparticle still inhibited the growth of the primary and metastatic tumors, especially i.p. metastases, we observed more heterogeneous response among tumors in the targeted treatment group (**Figure S3**). Following six treatments, residual tumors from four representative mice in the same treatment group that showed 12 to 86% of inhibition in tumor growth compared to the no-treatment control were analyzed for optical signal and theranostic IONP delivery. Our result showed that mouse M5 had the largest tumor and the strongest optical signal (**Figure 5D**). A high level of HER2 was detected in the primary tumor. High levels of IONPs were also found in both primary and metastatic tumors (**Figure 5E**). Therefore, it seemed that the residual tumor in this mouse had an adequate level of nanoparticle drug delivery, but the concentration of cisplatin was not sufficient to overcome intrinsic drug resistance in those tumor cells. Accumulation of a high level of NIR-830 dye-labeled theranostic IONPs without efficient tumor cell killing resulted in a strong signal for optical imaging of drug-resistant tumors. Mouse M4 showed intermediate growth inhibition and its residual tumors had low levels of HER2 and IONP drug accumulation. A relatively low level of optical signal was detected in the tumor (**Figure 5D-E**). Although there was a good response (72% of inhibition) in the primary tumor of mouse M6, resistant tumor cells surrounding a central necrotic

area had a high level of HER2. Intermediate levels of IONPs and optical signal were found in this tumor (**Figure 5D-E**). Finally, mouse M7 had the best response among all treated mice. A very small residual tumor in this mouse had a strong optical signal, suggesting that efficient nanoparticle drug delivery and high sensitivity of tumor cells to the therapy contributed to a good response at a lower cisplatin dose (**Figure 5D-E**).

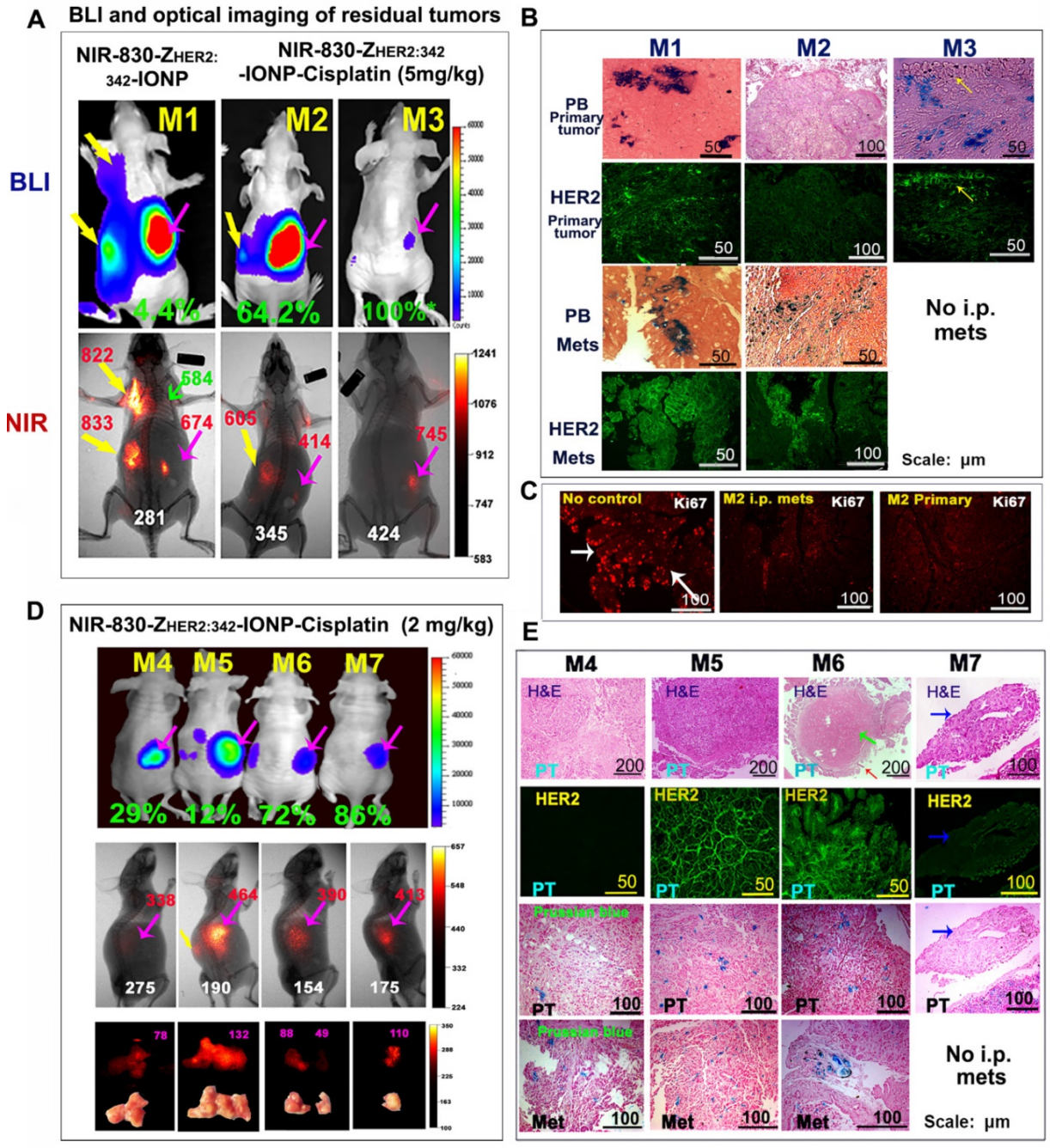

Figure 5. Correlation of differential therapeutic responses, optical signals and the levels of HER2 expression in drug resistant tumors. (A) BLI and optical imaging of residual tumors following the sixth treatment at 5 mg/kg cisplatin dose. BLI signal quantification: NIR-830-$Z_{HER2:342}$-IONP-Cisplatin treated mouse M2 ($1.4x10^8$ photon/second) and mouse M3 ($1.6x10^6$ photon/second). NIR-830-$Z_{HER2:342}$-IONP (no drug) treated mouse M1 ($2.5x10^9$ photon/second). Lung and i.p. metastases (yellow arrows); primary tumor (pink arrows). Green arrow: normal lung. **(B)** Prussia blue staining (PB) and immunofluorescence labeling. Higher levels of IONPs were detected in i.p. metastases compared to primary tumors. Mouse M2 lacked HER2 and IONP accumulation in the primary tumor and had a low level of HER2 in most metastatic tumor cells except in a subpopulation. Mouse M3 had IONP positive cells and a low level of HER2+ cells in a microscopic residual primary tumor. **(C)** Cell proliferation (Ki67+, red) in both primary and metastatic tumors was inhibited in mouse M2. **(D)** BLI and optical imaging of mice treated with a 2 mg/kg cisplatin dose of NIR-830-$Z_{HER2:342}$-IONP-Cisplatin. **(E)** Residual tumors of mouse M4 and M5 had dense tumor cells in H&E images. Primary tumor in mouse M4 lacked HER2 and had a low level of IONPs. A poor responder mouse M5 had high levels of HER2 and IONPs in the tumor. Mouse M6 had large necrotic areas (green arrow) in the primary tumor, while having viable HER2+ and IONP positive tumor cells at the tumor edge (red arrow). A good responder mouse M7 had a small and HER2 low expressing residual tumor. **A and D:** Green numbers: the percentages of tumor growth inhibition based on the tumor weight of no treatment control mice as 0%. Red numbers: optical intensity in tumors. White numbers: body background. Pink numbers: optical signal intensity measured on tumors by *ex vivo* imaging.

Significant inhibition of the development of tumor metastases following systemic, targeted therapy

One of the major advantages of systemic, targeted therapy is to treat disseminated tumor cells locally or in distant organs. The SKOV3 cell line-derived orthotopic tumor model has a high incidence of lung metastases. Six weeks after ovarian implantation of tumor cells, BLI revealed that all mice had developed lung and peritoneal metastases in the control group (**Figure 6A**). However, upon completing six targeted therapies using NIR830-$Z_{HER2:342}$-IONP-Cisplatin, we observed not only significant reduction of the primary tumors but also no detectable lung metastases in the mice by BLI examination and histological analysis (**Figure 6A-B** and **Figure S8**). Only one mouse had small peritoneal metastases. H&E staining of the lung tissues further confirmed the absence of lung metastases (**Figure 6B**).

Mice treated with cisplatin and non-targeted IONP-Cisplatin also had decreased lung metastases (**Figure 6A-B**). However, H&E-stained lung tissue sections revealed the presence of micrometastases (**Figure 6B** and **Figure S8**). All mice in the aforementioned two control groups also had detectable peritoneal metastases. Furthermore, Prussian blue staining demonstrated targeted delivery of NIR-830-$Z_{HER2:342}$-IONP-Cisplatin into HER2-expressing lung metastases in mice treated with either 2 or 5 mg/kg cisplatin dose of NIR-830-$Z_{HER2:342}$-IONP-Cisplatin (**Figure 6C**).

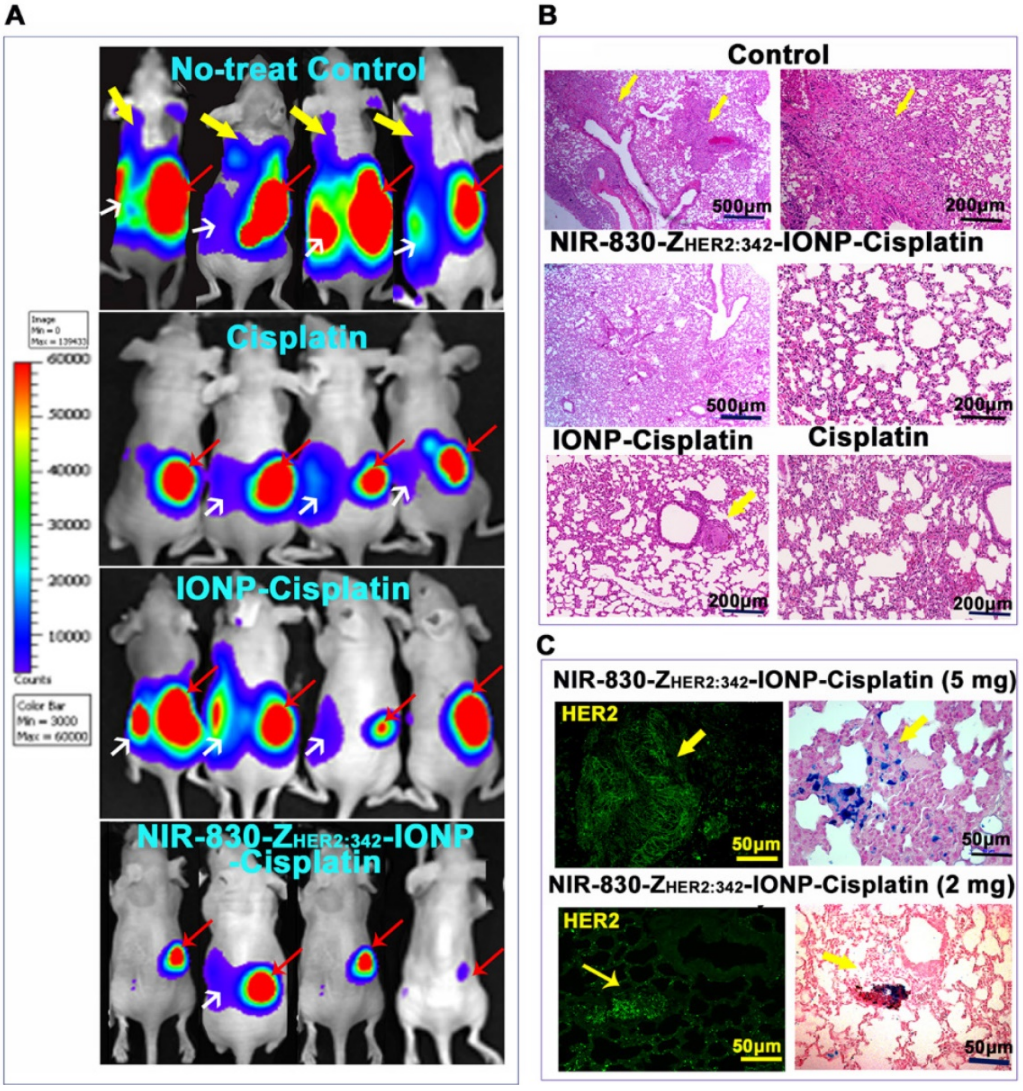

Figure 6. Systemic delivery of HER2-targeted theranostic IONP-Cisplatin inhibited the growth of metastatic tumors in orthotopic human ovarian cancer model. (A) BLI shows the presence of lung and i.p. metastases in all no-treatment control mice (upper panel). Six i.v. injections of a 5 mg/kg cisplatin equivalent dose of NIR-830-$Z_{HER2:342}$-IONP-Cisplatin markedly inhibited the lung and i.p. metastases (bottom panel). Mice treated with unconjugated cisplatin or non-targeted IONP-Cisplatin also showed inhibition of lung metastasis but still had large i.p. metastases and primary tumors. Red arrows: primary tumors; White arrows: i.p. metastases; Yellow arrows: lung metastases. **(B)** H&E staining of lung tissue sections from different groups. Large metastatic tumors were detected in the lungs of no-treatment control mice but none in mice treated with targeted IONP-Cisplatin. Low (100x) and high magnification (200x) microscopic images of the lung are shown. Small metastatic lesions were seen in the lung of the mice treated with non-targeted IONP-Cisplatin. A few lung metastatic lesions were seen in cisplatin-treated mice. **(C)** Immunofluorescence labeling and Prussian blue staining of serial tissue sections detected targeted delivery of NIR-830-$Z_{HER2:342}$-IONP-Cisplatin to HER2-expressing lung metastases (yellow arrows).

Detection of drug-resistant residual tumors using spectroscopic imaging

The inability to completely excise peritoneal metastases during surgery has been a major challenge for effective treatment of ovarian cancer patients [36]. We proposed that pre-operative therapy using targeted theranostic nanoparticles offers the opportunity to reduce the tumor burden, making complete surgical resection feasible. Accumulation of NIR-830-$Z_{HER2:342}$-IONP-Cisplatin in drug-resistant tumors enabled the detection of tumor lesions by optical imaging (**Figure 7A**). For intraoperative imaging, a handheld imaging device has been developed (**Figure S9**) [31], which sensitively detects spectroscopic and NIR signals of NIR-dye-conjugated IONPs. First, we examined the sensitivity of spectroscopic and NIR optical imaging of different drug-resistant primary tumors. Following the sixth treatment using NIR-830-$Z_{HER2:342}$-IONP-Cisplatin (5 mg/kg), various tumor responses were seen in the mice. In a mouse that showed a very weak BLI signal but no visible residual tumor in the ovary, both spectroscopic and NIR signals were detected in the orthotopic site, suggesting the ability to detect very small resistant tumors that contained theranostic IONPs (**Figure 5** and **Figure 7A;** mouse M3). A slightly higher signal was detected in a resistant tumor with 63% growth inhibition. As a delivery control, a large tumor in a mouse that received six injections of NIR-830-$Z_{HER2:342}$-IONPs but without carrying cisplatin to kill the nanoparticle-containing cells had the strongest spectroscopic and NIR signals (**Figure 7A**). Quantification of spectroscopic signals in three mice showed that the mean tumor signal was three-fold higher than the body background (**Figure 7B-C**).

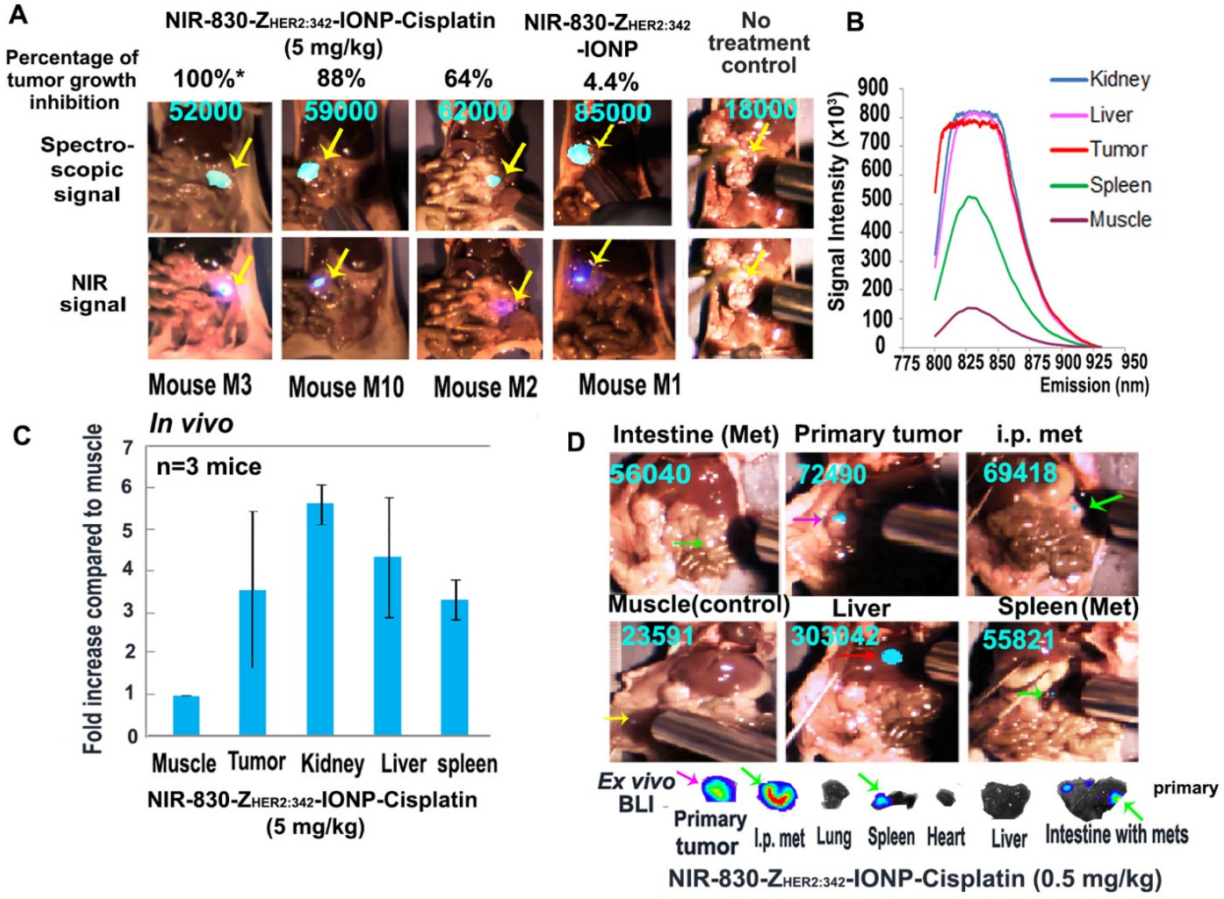

Figure 7. Detection of drug-resistant residual tumors in the peritoneal cavity using a handheld dual spectroscopic and NIR imaging device. (A) Spectroscopic signals in small and large drug-resistant residual tumors in mice treated with NIR-830-$Z_{HER2:342}$-IONP-Cisplatin (5 mg/kg). An intermediate level of spectroscopic signal was detected near the ovary in mouse M3 without a visible tumor. Delivery control: tumors treated with NIR-830-$Z_{HER2:342}$-IONP (no drug). Background control: basal signal in the tumor of no-treated control mouse. The percentage of tumor growth inhibition was calculated using the mean total tumor weight of no treatment control mice of 837 mg as 0% growth inhibition. Mouse M1: 800 mg (4.4%), mouse M2: 300 mg (64%), mouse M10: 100 mg (88%). Mouse M3: No visible tumor and only microscopic tumor (100%*). **(B)** Quantification of spectroscopic signals. The peak signal was at an emission wavelength of 830 nm. Tumor signal is 7 times higher than that in the muscle. Nonspecific signals in the liver and kidney were detected. **(C)** The mean spectroscopic signal intensity detected from three mice. All small and large tumors had signal intensity 2 to 5 times over the muscle background. The error bars are standard deviations from one measurement on each organ of three mice. **(D)** Detection of peritoneal metastatic tumors on the surface of normal organs. Despite a low dose of theranostic IONPs (0.5 mg/kg cisplatin), spectroscopic imaging detected strong signals in the primary (pink arrow) and metastatic tumors (green arrows). Several small tumor nodules on the surface of the intestine and spleen identified by *ex vivo* BLI (green arrows) had spectroscopic imaging signals two-fold higher than muscle background (yellow arrows). Red arrow: liver nonspecific signal.

To determine whether optical imaging was able to detect drug-resistant metastatic tumors in the peritoneal cavity, we used the mice treated with 0.5 mg/kg of cisplatin equivalent dose of NIR-830-$Z_{HER2:342}$-IONP-Cisplatin that had more peritoneal metastatic tumors than that treated with higher doses. As shown in **Figure 7D**, primary tumor and peritoneal metastases had about three-fold higher spectroscopic signal compared to the body background. As expected, high signal levels were found in the liver and kidney. Although some areas in the intestine had intermediate signals, we used a three-fold increase over the muscle signal as a cutoff for spectroscopic imaging (**Figure 7D** and **Figure S9**). One potential problem using this cutoff might be a low sensitivity of detection of small tumors on the surface of the liver and kidneys due to a high background signal resulting from nonspecific uptake of the nanoparticle drug by macrophages in the liver and clearance of the NIR dye by the kidneys. Among small metastatic deposits on the surface of the normal organs that were identified by *ex vivo* BLI, spectroscopic signals were approximately 2.3-fold higher than the body background. Thus, it is possible to detect small tumors on the surface of normal organs in the peritoneal cavity using a 2-fold increase as the cutoff value (**Figure 7D**). Our results clearly suggested that spectroscopic imaging can detect NIR-830-labeled theranostic IONPs in small residual tumors in the peritoneal cavity. Therefore, there is a potential for further development of image-guided surgery to improve current surgical management of ovarian cancer.

Discussion

Despite advances in drug development, resistance to therapy is still a daunting challenge. Human cancer is highly heterogeneous in its tumor vasculature as well as tumor cells and stromal components, leading to heterogeneous responses to therapeutic agents within the same tumor and among different tumor lesions in the same and different cancer patients. To the best of our knowledge, there is currently no reliable biomarker or prognostic factor to predict if a tumor will respond to a given therapeutic agent. Increasing evidence shows that biomarker-targeted nanoparticle drugs have improved delivery to tumors, leading to enhanced therapeutic response. Multifunctional theranostic nanoparticles that target a biomarker highly expressed in tumor cells for selective drug delivery, with the ability to monitor drug delivery and response to therapy, are promising nanotheranostic systems for the development of image-guided cancer therapy of heterogeneous and drug-resistant human cancers [23-26]. The unique properties of the HER2-targeted theranostic nanoparticle developed and validated in this study provide means for the development of a precision oncology protocol for effective treatment of cancer patients with HER2+ drug-resistant tumors (**Figure 1A**). Proof-of-concept studies in animal tumor models have the potential for the development of other biomarker-targeted theranostic nanoparticles for the treatment of human cancers.

In this study, we have demonstrated an enhanced delivery of nanoparticle drug into primary ovarian tumor as well as peritoneal and distant metastases using HER2-targeted theranostic IONP carrying cisplatin, which led to substantial tumor growth inhibition (88% inhibition at 5 mg/kg dose compared to no-treatment control) in an orthotopic human ovarian cancer xenograft model. A strong therapeutic response in metastatic tumors supported the potential of this targeted therapy for the treatment of metastatic HER2+ ovarian tumors. The use of a metastatic ovarian cancer model in nude mice having multiple tumor lesions with different levels of HER2 expression allowed for determining the feasibility of the application of non-invasive imaging for the detection of differential nanoparticle drug delivery and therapeutic response in those tumors.

Extensive efforts have been made to develop various targeted nanoparticle drug carriers [37, 38]. HER2 is a well-characterized biomarker for the development of targeted therapeutics, despite its heterogeneous levels of expression in human cancer [39]. Therefore, the ability to correlate the level of HER2 expression in tumor cells with delivery efficiency and therapeutic efficacy of HER2-targeted theranostic nanoparticles by non-invasive imaging and histological analysis should provide a critical information on the mechanisms of differential therapeutic responses in tumor cells that would have significance in future clinical applications. In comparison with other nanoparticle-based drug carriers (liposomes and polymeric nanoparticles), IONPs retained in drug-resistant tumor cells for longer durations, which made it possible to monitor nanoparticle drug delivery in tumors by non-invasive imaging and to determine therapeutic response by imaging individual tumor lesions. Such an approach can be used to investigate the causes of resistance to targeted therapy in tumor cells by histological analysis of individual tumors after preoperative, targeted therapy followed by surgical resection.

Our results confirmed that HER2 targeting played a major role in nanoparticle delivery and retention. A higher level of HER2 in tumor cells led to more theranostic IONPs to be delivered to metastatic tumors compared to primary tumors. Since tumor

endothelial cells do not overexpress HER2, it is likely that targeted or non-targeted IONP-Cisplatin were delivered into the tumor via the enhanced permeability and retention (EPR) effect. However, non-targeted-IONP-Cisplatin had a low drug delivery efficiency into tumor cells due to the lack of tumor retention. Those nanoparticle-based drug carriers retained in the interstitial space and stroma areas that were slightly acidic (pH 6.5 to 7) and not sufficient for cisplatin release, which occurred at pH 5 to 6. Some nanoparticles could be eliminated from the tumor by the lymphatic system or tumor vessels. Thus, an intermediate therapeutic response was seen in mice treated with IONP-Cisplatin. On the other hand, without a high level of HER2 on tumor cells, targeted theranostic IONP could not effectively enter tumor cells. Subsequently, they also had low accumulation in the tumor, leading to poor to modest therapeutic responses. Demonstration of HER2-targeted delivery of the IONPs into peritoneal and distant metastases and significant growth inhibition of metastatic tumors suggest the potential of this targeted therapy for the treatment of metastatic HER2+ tumors. Non-invasive MRI of tumor growth inhibition and drug-resistant tumors offers an opportunity for further translational development of this integrated, image-guided cancer therapy platform for the treatment of HER2+ tumors, especially advanced ovarian cancer.

At present, there is no adequate non-invasive approach to evaluate targeted drug delivery and response to therapy in human cancers that have different levels of biomarker expression and therapeutic response. Even when biopsy could be performed to obtain tumor tissue samples, the result only represents a specific tumor area, but is unable to provide the expression level of a biomarker and analysis of delivery of therapeutic agents in the entire tumor and in different tumors in the same patient. Moreover, many metastatic tumors are not accessible for biopsy. Therefore, the ability of non-invasive imaging to efficiently visualize nanoparticle drug delivery and changes in tumor volume should provide a valuable information for the development of personalized treatment and for improvement of therapeutic response in heterogeneous cancer.

Increasing evidence supports the feasibility of developing magnetic IONP-based drug carriers for clinical translation due to its biodegradable and biocompatible nature and relatively high capacity for drug loading [40]. Several non-targeted IONPs have been used for MRI of lymph node metastases and liver cancer in humans, or for the treatment of severe anemia in patients with chronic kidney diseases [41-43]. Compared to other theranostic agents, magnetic IONPs have a translational advantage in their ability to be detected by a clinical 3-T MRI scanner**.** MRI, in combination with targeted delivery of theranostic IONPs, should be a good clinical imaging modality since it offers excellent quantitative imaging and 4-D imaging capacity for tumor lesions located deep in the peritoneal cavity. In this study, we found that systemic delivery of NIR-830-$Z_{HER2:342}$-IONP-Cisplatin led to marked MRI T_2 signal intensity decrease in small and large ovarian tumors. While T_2 mapping method can be readily adopted to clinical imaging protocols, we also realize that the detection of magnetic IONP theranostic agents in tumors based on a decrease in T_2 signal intensity, or the "negative-contrast" effect, has a limitation in specificity and sensitivity when studying an abnormal area that has low background signals from surrounding organs, e.g. the intestine, liver or spleen. However, an alternative ultrashort echo time (UTE) imaging that allows for obtaining T_1-weighted "positive or bright" contrast enhancement from magnetic IONPs can be used as demonstrated in our prior study [44, 45]. Our previous study also showed that the combination of multimodality imaging approaches, such as 3D fluorescence tomography, photoacoustic and MR imaging, with NIR-830 dye-labeled HER2-targeted IONPs could improve the detection of ovarian tumors in the peritoneal cavity [27, 46].

At present, the standard therapy for advanced ovarian cancers is debulking surgery followed by i.v. platinum and taxane chemotherapy [47, 48]. Current surgery for ovarian cancer has a major unmet challenge of the inability to completely excise of all tumor nodules on the surface of normal organs in the peritoneal cavity. The guideline of optimal debulking surgery has been defined as the diameter of the largest residual tumor nodule that remains after surgery is 1 cm or less [36, 49]. Despite the combination of surgery and chemotherapy, most patients will ultimately develop recurrent tumors and the ten-year survival rates for ovarian cancer patients with the stage III and IV diseases are 21% and less than 5%, respectively [47]. It is likely that preoperative, targeted therapy using theranostic nanoparticles has the potential to significantly reduce tumor burdens in primary tumor as well as peritoneal and distant tumor metastases, which could pave the way for a more complete debulking surgery using optical image-guided surgery to remove drug-resistant residual tumors [50]. Such an integrated therapy using a precision oncology protocol has the potential to improve outcome of the treatment for advanced ovarian cancer patients.

Abbreviations

BLI: bioluminescence imaging, BSA: bovine serum albumin, FDA: Food and Drug Administration, FOV: field-of-view, HER2: human epidermal growth factor receptor 2, HRP: horseradish peroxidase, IONP: iron oxide nanoparticle, i.p.: intraperitoneal, Met: metastatic tumor, MRI: magnetic resonance image, NIR: near-infrared fluorescence, NIR-830-$Z_{HER2:342}$-IONP-Cisplatin: Near-infrared 830 dye-labeled HER2 affibody ($Z_{HER2:342}$) conjugated magnetic iron oxide nanoparticle carrying cisplatin, pmol: picomolar, PT: primary tumor, ROIs: regions of interest, TE: echo time, TR: repetition time.

Supplementary Material

Supplementary figures.
http://www.thno.org/v09p0778s1.pdf

Acknowledgements

We thank Dr. Daniela Matei at Indiana University-Purdue University (Currently, Professor at Feinburg School of Medicine, NWU) for providing SKOV3-Luc cell line, Dr. Neil Sidell for providing OVCAR3 cell line, Dr. Nelson Chen for assisting in statistical analysis, Dr. Yaolin Xu for conducting transmission electron microscopy study, and Dr. Mohammad Raheel Jajja for editing the manuscript. This work was supported by the following NIH/NCI awards: R01CA133722-01, R01CA154846-01, R01 CA202846-01, R01CA163256-01, and NCI Cancer Nanotechnology partnership Platform (NIH, U01 CA151810), NIH K99/R00153916, and the Nancy Panoz Endowed Chair to Dr. Lily Yang.

Competing interests

Dr. Y. Andrew Wang is the President and Principal Scientist at Ocean Nanotech LLC, San Diego, CA. All other authors have declared that no conflict of interest exists.

References

1. Scott AM, Wolchok JD, Old LJ. Antibody therapy of cancer. Nat Rev Cancer. 2012; 12:278-87.
2. Talavera A, Friemann R, Gomez-Puerta S, Martinez-Fleites C, Garrido G, Rabasa A, et al. Nimotuzumab, an antitumor antibody that targets the epidermal growth factor receptor, blocks ligand binding while permitting the active receptor conformation. Cancer Res. 2009; 69:5851-9.
3. Sievers EL, Senter PD. Antibody-drug conjugates in cancer therapy. Annu Rev Med. 2013; 64:15-29.
4. Baselga J, Cortes J, Kim SB, Im SA, Hegg R, Im YH, et al. Pertuzumab plus trastuzumab plus docetaxel for metastatic breast cancer. N Engl J Med. 2012; 366:109-19.
5. Swain SM, Clark E, Baselga J. Treatment of HER2-positive metastatic breast cancer. N Engl J Med. 2015; 372:1964-5.
6. Seol H, Lee HJ, Choi Y, Lee HE, Kim YJ, Kim JH, et al. Intratumoral heterogeneity of HER2 gene amplification in breast cancer: its clinicopathological significance. Mod Pathol. 2012; 25:938-48.
7. Lewis JT, Ketterling RP, Halling KC, Reynold C, Jenkins RB, Visscher DW. Analysis of intratumoral heterogeneity and amplification status in breast carcinomas with equivocal (2+) HER2 immunostaining. Am J Clin Pathol. 2005;124:273-81.
8. Rubin SC, Finstad CL, Federici MG, Scheiner L, Lloyd KO, Hoskins WJ. Prevalence and significance of HER2/Neu expression in early epithelial ovarian cancer. Cancer. 1994; 73:1456-59.
9. Meijer SL, Wesseling J, Smit VT, Nederlof PM, Hooijer GK, Ruijter H, et al. HER2 gene amplification in patients with breast cancer with equivocal IHC results. J Clin Pathol. 2011; 64:1069-72.
10. Bookman MA, Darcy KM, Clarke-Pearson D, Boothby RA, Horowitz IR. Evaluation of monoclonal humanized anti-HER2 antibody, trastuzumab, in patients with recurrent or refractory ovarian or primary peritoneal carcinoma with overexpression of HER2: a phase II trial of the Gynecologic Oncology Group. J Clin Oncol. 2003; 21:283-90.
11. Gordon MS, Matei D, Aghajanian C, Matulonis UA, Brewer M, Fleming GF, et al. Clinical activity of pertuzumab (rhuMAb 2C4), a HER dimerization inhibitor, in advanced ovarian cancer: potential predictive relationship with tumor HER2 activation status. J Clin Oncol. 2006; 24:4324-32.
12. Kelland L. The resurgence of platinum-based cancer chemotherapy. Nat Rev Cancer. 2007; 7:573-84.
13. Raja FA, Chopra N, Ledermann JA. Optimal first-line treatment in ovarian cancer. Ann Oncol. 2012; 23 Suppl 10:x118-27.
14. Tapia G, Diaz-Padilla I. Molecular mechanisms of platinum resistance in ovarian cancer. In Díaz-Padilla I, Ed. Ovarian cancer - a clinical and translational update. Croatia: InTech; 2013:205-23.
15. Uchino H, Matsumura Y, Negishi T, Koizumi F, Hayashi T, Honda T, et al. Cisplatin-incorporating polymeric micelles (NC-6004) can reduce nephrotoxicity and neurotoxicity of cisplatin in rats. Br J Cancer. 2005; 93:678-87.
16. Shi J, Kantoff PW, Wooster R, Farokhzad OC. Cancer nanomedicine: progress, challenges and opportunities. Nat Rev Cancer. 2017; 17:20-37.
17. Yap TA, Carden CP, Kaye SB. Beyond chemotherapy: targeted therapies in ovarian cancer. Nat Rev Cancer. 2009; 9:167-81.
18. Ren Y, Cheung HW, von Maltzhan G, Agrawal A, Cowley GS, Weir BA, et al. Targeted tumor-penetrating siRNA nanocomplexes for credentialing the ovarian cancer oncogene ID4. Sci Transl Med. 2012; 4:147ra12.
19. Paraskar AS, Soni S, Chin KT, Chaudhuri P, Muto KW, Berkowitz J, et al. Harnessing structure-activity relationship to engineer a cisplatin nanoparticle for enhanced antitumor efficacy. Proc Natl Acad Sci U S A. 2010; 107:12435-40.
20. Dhar S, Kolishetti N, Lippard SJ, Farokhzad OC. Targeted delivery of a cisplatin prodrug for safer and more effective prostate cancer therapy *in vivo*. Proc Natl Acad Sci U S A. 2011;108:1850-5.
21. Xiao K, Li Y, Lee JS, Gonik AM, Dong T, Fung G, et al. "OA02" peptide facilitates the precise targeting of paclitaxel-loaded micellar nanoparticles to ovarian cancer *in vivo*. Cancer Res. 2012; 72:2100-10.
22. Peer D, Karp JM, Hong S, Farokhzad OC, Margalit R, Langer R. Nanocarriers as an emerging platform for cancer therapy. Nat Nanotechnol. 2007; 2:751-60.
23. Chen HM, Zhang WZ, Zhu GZ, Xie J, Chen XY. Rethinking cancer nanotheranostics. Nat. Rev. Mater. 2017; 2:17024.
24. Lin J, Wang M, Hu H, Yang X, Wen B, Wang Z, et al. Multimodal-imaging-guided cancer phototherapy by versatile biomimetic theranostics with UV and gamma-irradiation protection. Adv Mater. 2016; 28:3273-9.
25. Zhou H, Qian W, Uckun FM, Wang L, Wang YA, Chen H, et al. IGF1 receptor targeted theranostic nanoparticles for targeted and image-guided therapy of pancreatic cancer. ACS Nano. 2015; 9:7976-91.
26. Li Y, Lin TY, Luo Y, Liu Q, Xiao W, Guo W, et al. A smart and versatile theranostic nanomedicine platform based on nanoporphyrin. Nat Commun. 2014; 5:4712.
27. Satpathy M, Wang L, Zielinski R, Qian W, Lipowska M, Capala J, et al. Active targeting using HER2-affibody-conjugated nanoparticles enabled sensitive and specific imaging of orthotopic HER2 positive ovarian tumors. Small. 2014; 10:544-55.
28. Lee SB, Hassan M, Fisher R, Chertov O, Chernomordik V, Kramer-Marek G, et al. Affibody molecules for *in vivo* characterization of HER2-positive tumors by near-infrared imaging. Clin Cancer Res. 2008; 14:3840-9.
29. Zhou Z, Chen H, Lipowska M, Wang L, Yu Q, Yang X, el al. A dual-modal magnetic nanoparticle probe for preoperative and intraoperative mapping of sentinel lymph nodes by magnetic resonance and near infrared fluorescence imaging. J Biomater Appl. 2013; 28:100-11.
30. Golla ED, Ayres GH. Spectrophotometric determination of platinum with o-phenylenediamine. Talanta. 1973; 20:199-210.
31. Mohs AM, Mancini MC, Singhal S, Provenzale JM, Leyland-Jones B, Wang MD, et al. Hand-held spectroscopic device for *in vivo* and intraoperative tumor detection: contrast enhancement, detection sensitivity, and tissue penetration. Anal Chem. 2010; 82:9058-65.
32. Shen Z, Wu A, Chen X. Iron oxide nanoparticle based contrast agents for magnetic resonance imaging. Mol Pharm. 2017; 14:1352-64.
33. Yen SK, Padmanabhan P, Selvan ST. Multifunctional iron oxide nanoparticles for diagnostics, therapy and macromolecule delivery. Theranostics. 2013; 3:986-1003.
34. Li K, Nejadnik H, Daldrup-Link HE. Next-generation superparamagnetic iron oxide nanoparticles for cancer theranostics. Drug Discov Today. 2017; 22:1421-9.
35. Blanco E, Shen H, Ferrari M. Principles of nanoparticle design for overcoming biological barriers to drug delivery. Nat Biotechnol. 2015; 33:941-51.

36. Palmirotta R, Silvestris E, D'Oronzo S, Cardascia A, Silvestris F. Ovarian cancer: Novel molecular aspects for clinical assessment. Crit Rev Oncol Hematol. 2017; 117:12-29.
37. Bar-Zeev M, Livney YD, Assaraf YG. Targeted nanomedicine for cancer therapeutics: Towards precision medicine overcoming drug resistance. Drug Resist Updat. 2017; 31:15-30.
38. Miao L, Guo S, Lin CM, Liu Q, Huang L. Nanoformulations for combination or cascade anticancer therapy. Adv Drug Deliv Rev. 2017; 115:3-22.
39. English DP, Roque DM, Santin AD. HER2 expression beyond breast cancer: therapeutic implications for gynecologic malignancies. Mol Diagn Ther. 2013; 17:85-99.
40. Miller MA, Gadde S, Pfirschke C, Engblom C, Sprachman MM, Kohler RH, et al. Predicting therapeutic nanomedicine efficacy using a companion magnetic resonance imaging nanoparticle. Sci Transl Med. 2015; 7:314ra183.
41. Wang YX, Idee JM. A comprehensive literatures update of clinical researches of superparamagnetic resonance iron oxide nanoparticles for magnetic resonance imaging. Quant Imaging Med Surg. 2017; 7:88-122.
42. Pai AB, Garba AO. Ferumoxytol: a silver lining in the treatment of anemia of chronic kidney disease or another dark cloud? J Blood Med. 2012; 3:77-85.
43. Thakor AS, Jokerst JV, Ghanouni P, Campbell JL, Mittra E, Gambhir SS. Clinically Approved Nanoparticle Imaging Agents. J Nucl Med. 2016; 57:1833-37.
44. Wang L, Zhong X, Qian W, Huang J, Cao Z, Yu Q, et al. Ultrashort echo time (UTE) imaging of receptor targeted magnetic iron oxide nanoparticles in mouse tumor models. J Magn Reson Imaging. 2014; 40:1071-81.
45. Lee GY, Qian WP, Wang L, Wang YA, Staley CA, Satpathy M, et al. Theranostic nanoparticles with controlled release of gemcitabine for targeted therapy and MRI of pancreatic cancer. ACS Nano. 2013;7:2078-89.
46. Xi L, Satpathy M, Zhao Q, Qian W, Yang L, Jiang H. HER2/neu targeted delivery of a nanoprobe enables dual photoacoustic and fluorescence tomography of ovarian cancer. Nanomedicine. 2014;10:669-77.
47. Jelovac D, Armstrong DK. Recent progress in the diagnosis and treatment of ovarian cancer. CA Cancer J Clin. 2011; 61:183-203.
48. Cannistra SA. Cancer of the ovary. N Engl J Med. 2004; 351:2519-29.
49. Tewari D, Java JJ, Salani R, Armstrong DK, Markman M, Herzog T, el al. Long-term survival advantage and prognostic factors associated with intraperitoneal chemotherapy treatment in advanced ovarian cancer: a gynecologic oncology group study. J Clin Oncol. 2015; 33:1460-6.
50. Mohs AM, Mancini MC, Provenzale JM, Saba CF, Cornell KK, Howerth EW, et al. An integrated wide-field imaging and spectroscopy system for contrast-enhanced, image-guided resection of tumors. IEEE Trans Biomed Eng. 2015; 62:1416- 24.